




Review

Neutron Scattering as a Powerful Tool to Investigate Magnetic Shape Memory Alloys: A Review

Natalia A. Río-López ¹, Patricia Lázpita ^{1,2}, Daniel Salazar ¹, Viktor I. Petrenko ^{1,3} , Fernando Plazaola ² , Volodymyr Chernenko ^{1,2,3}  and Jose M. Porro ^{1,3,*}

- ¹ BCMaterials, Basque Center for Materials, Applications & Nanostructures, 48940 Leioa, Spain; natalia.rio@bcmaterials.net (N.A.R.-L.); patricia.lazpita@ehu.eus (P.L.); daniel.salazar@bcmaterials.net (D.S.); viktor.petrenko@bcmaterials.net (V.I.P.); vladimir.chernenko@gmail.com (V.C.)
- ² Department of Electricity and Electronics, Faculty of Science and Technology, University of the Basque Country, 48080 Bilbao, Spain; fernando.plazaola@ehu.eus
- ³ Ikerbasque, Basque Foundation for Science, 48009 Bilbao, Spain
- * Correspondence: jm.porro@bcmaterials.net

Abstract: Magnetic shape memory alloys (MSMAs) are an interesting class of smart materials characterized by undergoing macroscopic deformations upon the application of a pertinent stimulus: temperature, stress and/or external magnetic fields. Since the deformation is rapid and contactless, these materials are being extensively investigated for a plethora of applications, such as sensors and actuators for the medical, automotive and space industries, energy harvesting and damping devices, among others. These materials also exhibit a giant magnetocaloric effect, whereby they are very promising for magnetic refrigeration. The applications in which they can be used are extremely dependent on the material properties, which are, in turn, greatly conditioned by the structure, atomic ordering and magnetism of a material. Particularly, exploring the material structure is essential in order to push forward the current application limitations of the MSMAs. Among the wide range of available characterization tools, neutron scattering techniques stand out in acquiring advanced knowledge about the structure and magnetism of these alloys. Throughout this manuscript, a comprehensive review about the characterization of MSMAs using neutron techniques is presented. Several elastic neutron scattering techniques will be explained and exemplified, covering neutron imaging techniques—such as radiography, tomography and texture diffractometry; diffraction techniques—magnetic (polarized neutron) diffraction, powder neutron diffraction and single crystal neutron diffraction, reflectometry and small angle neutron scattering. This will be complemented with a few examples where inelastic neutron scattering has been employed to obtain information about the phonon dispersion in MSMAs.

Keywords: magnetic shape memory alloys; neutron scattering; Heusler alloys



Citation: Río-López, N.A.; Lázpita, P.; Salazar, D.; Petrenko, V.I.; Plazaola, F.; Chernenko, V.; Porro, J.M. Neutron Scattering as a Powerful Tool to Investigate Magnetic Shape Memory Alloys: A Review. *Metals* **2021**, *11*, 829. <https://doi.org/10.3390/met11050829>

Academic Editors: Sergey Kustov and Thomas Niendorf

Received: 23 April 2021

Accepted: 14 May 2021

Published: 18 May 2021

Publisher's Note: MDPI stays neutral with regard to jurisdictional claims in published maps and institutional affiliations.



Copyright: © 2021 by the authors. Licensee MDPI, Basel, Switzerland. This article is an open access article distributed under the terms and conditions of the Creative Commons Attribution (CC BY) license (<https://creativecommons.org/licenses/by/4.0/>).

1. Introduction

Magnetic shape memory alloys (MSMAs) are an interesting class of smart materials exhibiting the martensitic transformation and/or twinning induced large macroscopic deformations upon the application of pertinent stimuli, such as temperature, stress and/or magnetic field (see, e.g., [1–4] and references therein). Since these deformations are rapid and contactless, these kinds of materials are being extensively investigated for plenty of potential applications [5,6]. The applications in which they can be used are crucially dependent of the material properties, these being greatly conditioned by their structure, atomic ordering and magnetic state [3,7]. Thus, exploring the crystal structure is essential in order to establish the current limits of these materials and their related interesting applications. As in the case of many other functional materials, magnetic shape memory alloys possess quite complex crystallographic nuclear and magnetic structures, and their determination by means of classic techniques (X-Ray Diffraction, Scanning and Transmission Electron

Microscopy, etc.) requires often to be complemented by more advanced characterization techniques. Among the possible solutions, neutron scattering stands out as an ideal probing tool to successfully determine the aforementioned crystal and magnetic structures [7–9]. In the present manuscript, after concise introductory notes about MSMA and neutron scattering techniques provided below, a brief review highlighting a remarkable effectiveness of neutrons in the studies of different MSMA is presented.

1.1. Magnetic Shape Memory Alloys, MSMA

Active materials, defined as those which generate a controllable response as a result of an external stimulus, are usually employed as sensors and actuators for various industrial applications. In these devices, the impulses that lead to the sensing or actuating capacities consist in some type of stimulus (thermal, electrical, etc.), while the response consists either in a deformation or in another type of useful reaction. Shape Memory Alloys (SMA) are well-known active materials characterized by a peculiar response, which consists in a thermally-induced recovering process of their original shape after suffering from a pseudoplastic deformation in the martensitic state: this is the conventional Shape Memory Effect, SME [10–12]. The so-called Martensitic Transformation (MT) is responsible for this effect. This structural first-order phase transformation is also responsible for many other interesting effects, such as the thermoelastic or the superelastic effects, among others. The MT involves a phase transition between two solid-state phases: the austenitic phase or austenite, which is a high symmetry, high temperature phase; and the martensitic phase or martensite, which is a low symmetry, low temperature phase. Due to the diffusionless character of the MT, both phases share the same chemical composition. The origin of the MT embodies a thermoelastic transformation, where a temperature change and/or the application of a mechanical stress leads to a change in the crystal structure of the alloy. This deformation implies a uniform lattice distortion characterized with an invariant distortive habit plane, resulting in the crystallographic correspondence between the martensitic and austenitic lattices. To minimize the elastic energy generated due to a strong shape change at the MT, the martensitic phase exhibits an inhomogeneous lattice invariant deformation by twinning. The crystallographically identical twin variants present in the martensite phase, initially randomly oriented when the thermally induced MT is accomplished, can be aligned upon the application of an external uniaxial stress that gives as a result the martensitic plasticity. Being a first-order transformation, the spontaneous MT is accompanied by a thermal hysteresis $\Delta T = T_A - T_M$, where T_A is the austenitic temperature characterizing the reverse MT obtained during heating, and T_M is the martensitic temperature corresponding to the forward MT obtained during cooling [10,13].

Magnetic Shape Memory Alloys (MSMA) are mostly Heusler-type alloys exhibiting MT and a conventional SME, as well as, due to their magnetic nature, Large Magnetic Field Induced Strains (MFIS) either as a result of microstructural changes in the martensitic state or triggered by the MT [4,14]. As a consequence, a possible classification of the Heusler-type MSMA can be established by dividing them in two groups: Ferromagnetic (FSMA) and Metamagnetic (MetaMSMA) Shape Memory Alloys [4,15].

Off-stoichiometric Ni_2MnGa Heusler alloys are the archetypical prototypes of FSMA. They exhibit MT from the ferromagnetic austenite to the ferromagnetic martensite with a small change in their saturation magnetization. In the martensitic state they show a highly mobile twin microstructure with the twinning stress which can be varied down to about 0.05 MPa [16]. Due to a strong magnetoelastic coupling in FSMA, the application of an external field close to the anisotropy field of the compound can produce equivalent uniaxial stress values of 1–3 MPa, large enough to drive the twin rearrangements resulting in the aforementioned large MFIS [4]. The schematic behavior of a FSMA depicted in Figure 1 shows an operation cycle of a single crystalline FSMA sample usually employed in commercially available devices. If the material is cooled below the MT temperature, T_M , a martensitic microstructure formed by crystallographically equivalent twin variants is obtained. The application of a magnetic field, H , increases the volume fraction of the

twin variants with their easy-magnetization short c -axis of the tetragonal unit cell aligned with the field, hence elongating the sample in the direction perpendicular to the applied field. Subsequently, a mechanical compressive stress, F , can be applied in order to reset the sample shape, as shown in Figure 1. The initial shape will be recovered by raising the temperature above T_A , i.e., returning to the austenite phase.

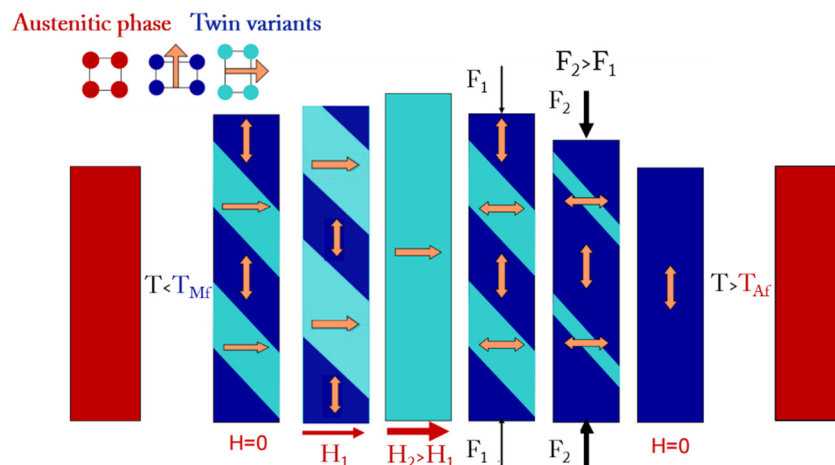


Figure 1. Schematic behavior of the process of the martensitic transformation, MT, magnetic field induced strain, MFIS, and the subsequent mechanical reset of the sample in a ferromagnetic shape memory alloy [17]. The sample is first cooled below T_M to transform from the austenite to a self-accommodated martensitic phase without applying any magnetic field ($H = 0$). The twin variants show different structural orientations and, consequently, different orientations of their magnetic moments (indicated by the orange arrows). When applying a magnetic field (H_1), the twin variants with the magnetic moments along the field grow at the expense of the others. By increasing the magnetic field (H_2), a full reorientation of the martensitic variants occurs and a single variant representing also a single magnetic domain state of the sample is reached, resulting in a macroscopic deformation. The inverse process until the former single variant state is induced by mechanical compression stress (F_1 , F_2). Further heating over T_A recovers the initial shape of the sample in the austenite phase. Reproduced from Ph.D. Thesis of A. Pérez-Checa, University of the Basque Country [17].

The functionality of these compounds strongly depends on the crystal structure of the martensitic phase, the transformation behavior, the magnetic and the elastic properties of the FSMAs, which are highly sensitive to the alloy composition, lattice defects and atomic ordering. This was reconfirmed recently during the development of high temperature Ni-Mn-Ga FSMAs [17,18].

Heusler-type MetaMSMAs, represented mostly by Mn-rich Ni-Mn-X ($X = \text{Sn, In, Sb}$) compounds [19,20], are characterized by strong competitive ferro-antiferro magnetic exchange interactions within the unit cell of the crystal lattice. They show MT from the ferromagnetic austenite to a weak magnetic (antiferromagnetic, superparamagnetic, ferromagnetic) martensite, which is accompanied by a huge abrupt change of the magnetization, a large specific volume change and latent heat. Contrary to FSMAs, the MT temperatures in MetaMSMAs are strongly dependent on the magnetic field enabling the magnetic field induced MT at constant temperature under the application of moderate magnetic fields. The magnetic field triggered MT gives rise to the large MFIS effect [21] or to the giant inverse magnetocaloric effect (IMCE) [22]. Whereas the study of the MFIS effect in these alloys is still at its infancy [4], the IMCE is currently subject of intensive world-wide investigations (see [15] and references therein) where, as in case of FSMAs, the composition, crystal and magnetic structures play a crucial role.

MSMAs can be utilized in several forms: single crystals, polycrystalline bulks, powders and thin films [23]. Single crystalline bulks are highly deformable in the martensitic

state, but they are difficult and expensive to produce. Polycrystalline MSMAs, cheap and technologically easily accessible, show much smaller MFIS capabilities than single crystals with similar compositions, due to constraints from the grain boundaries inhibiting the twin boundary motion [24–27]. Thin films, epitaxially grown on a substrate, exhibit many more constraints from the substrate that result into difficulties for them to show uniform deformations. Nonetheless, they are promising candidates, especially in cantilever or free-standing form, for their implementation in different industrial applications, such as Micro-Electro-Mechanical Systems (MEMS) and Micro-Magneto-Mechanical Systems (MMMS) [13,28,29].

1.2. Neutron Scattering Techniques

Neutron scattering techniques are widely used in materials science due to their versatility and multidisciplinary character, being the determination of the atomic relative positions and atom mobilities in solid or liquid bulk materials one possible application example of these techniques. The basis of neutron scattering consists in the measurement of the intensity of a neutron scattered beam after the beam has passed through the sample. Neutrons possess no charge and their electric dipole is zero, one of the reasons why they can penetrate matter far deeper than charged particles. This, along with the fact that neutrons interact with atoms via nuclear rather than electrical forces, and because nuclear forces are very short ranged, allows neutrons to travel large distances through most materials without being adsorbed or scattered. The interactions between neutrons and atomic nuclei allow them to differentiate isotopes and nearby elements in the periodic table, which is an advantage over other techniques such as X-ray or electron diffraction. Neutrons can probe not only the nuclear structure of materials, but also their magnetic properties. This is a consequence of the fact that neutrons possess a net magnetic moment, so they interact magnetically with the electrons in the sample, resulting in magnetic scattering events whose analysis yields specific information about the magnetic structure of the sample [17,30].

Especially in the case of the Heusler type Ni-X-Y (X,Y = Mn, Ga, Sn, In, Sb, Fe) MSMAs, neutron scattering has a much better precision in the determination of chemical ordering compared to X-ray diffraction. This is due to the very different neutron scattering lengths between elements that have similar Z number, as they are independent of the atomic number Z [31]. The differences in the scattering lengths between neutron and X-ray scattering events in elements commonly employed in MSMAs are shown schematically in Figure 2.

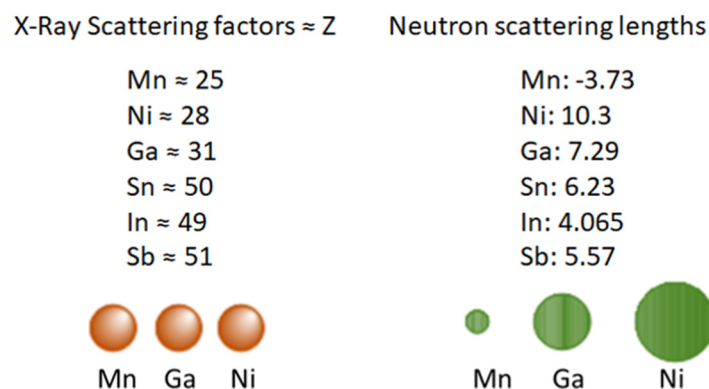


Figure 2. X-ray scattering form factors and neutron scattering lengths of several elements commonly found in Heusler type alloys. A visual comparison of these is shown for Ni-Mn-Ga FSMA.

Neutron scattering techniques can be classified in two large groups: elastic and inelastic, usually employed to probe the structure and the lattice dynamics, respectively, of the materials being investigated. The former group does not imply energy exchange between the neutrons and atoms in the sample, while the latter does. Even if inelastic neutron scattering remains an almost unexplored terrain to study MSMAs, this review

presents a few studies where these techniques have been employed in these materials, together with a comprehensive recompilation of studies that make use of elastic neutron scattering to probe MSMA.

Among the elastic neutron scattering techniques, three subgroups appear: neutron imaging (radiography/tomography and texture diffractometry), large scale structures (reflectometry and small-angle scattering) and diffraction (both in powder and in single crystal), all of them including polarized (magnetic structure) and non-polarized (nuclear structure) neutron scattering experiments. As already mentioned, MSMA usually present complex crystallographic nuclear and magnetic structures, so their properties are greatly conditioned by the crystal structure and atomic ordering. As an example, two alloys with the same composition can exhibit different transformation and magnetic characteristics if the atoms in the unit cell are arranged in a different way. In order to predict how a specific alloy will behave, a profound understanding of the exact atomic ordering is crucial, an aspect in which neutron scattering techniques excel in MSMA. In this framework, several situations in which each of the aforementioned techniques have been employed to characterize MSMA are reviewed hereafter [17,30,32,33].

Neutron scattering techniques provide scientists investigating MSMA with unique tools to access information in these alloys that cannot be accessed anyhow else, as it is the case of obtaining not only the atomic site occupancies, but also the magnetic site densities with majestic precision. Moreover, the presence of inhomogeneities in the bulk samples, both structural and magnetic, can uniquely be determined by neutron scattering and cannot be explored by any other technique. These unique capabilities demonstrated by neutron scattering techniques compensate the efforts needed to access neutron sources, where neutron beam times are awarded to scientists upon the presentation of a beam time proposal, which is evaluated by a panel of experts and by the local scientists of the neutron sources.

2. Elastic Neutron Scattering Studies of MSMA

2.1. Diffraction

2.1.1. Powder Neutron Diffraction

Powder diffraction is the neutron scattering technique employed when the crystal structure of powder samples needs to be explored [34,35]. It is used to detect and identify crystalline phases, to quantitatively determine their lattice parameters and volume fractions and, in general, to characterize atomic arrangements and the microstructure of polycrystalline materials in powder form. There are two types of powder neutron diffraction methods: angle-dispersive and energy-dispersive. In the conventional method of neutron powder diffraction, also known as angle-dispersive or fixed-wavelength, neutrons of a fixed wavelength are selected by a crystal monochromator. These neutrons are then scattered by the sample and the intensity $I(\theta)$ of the scattered beam is measured as a function of the scattering angle 2θ . An experimental plot of $I(\theta)$ vs. θ shows diffractions peaks whose positions are determined by the Bragg law $n\lambda = 2d\sin\theta$, where d is the interplanar spacing between the different lattice planes of the crystal structure, n is an integer number and λ is the neutron wavelength. By reversing the roles of θ and λ , it is possible to measure the intensity $I(\lambda)$ vs. λ at a fixed value of 2θ . This is the fixed-angle or energy-dispersive method. In the first method, the “white” (non-monochromatic) neutron beam from the reactor passes through a collimator in the reactor shield, and a particular wavelength is then selected by a crystal monochromator, as previously mentioned. In the latter, the wavelength of the neutrons is determined by measuring the time it takes for them to reach the detector: this is the so-called time-of-flight neutron scattering method [32,33,36,37].

Neutron powder diffraction has historically been used to study Ni-Mn-Ga FSMA. Back in the early 1980s, Webster et al. [38] employed neutron powder diffraction to study the structure and the structural phase transformations of a stoichiometric Ni₂MnGa Heusler alloy. These measurements played an important role in confirming that the crystal structure is highly L₂₁-ordered, schematically represented in Figure 3, and that the structural trans-

formation turns out to be reversible during cooling-heating cycles. In the early 2000s, the growing interest in these alloys led to the occurrence of several neutron powder diffraction studies in off-stoichiometric and doped Ni-Mn-Ga FSMAs. High resolution powder neutron diffraction was used by Brown et al. [39] to study the martensitic and premartensitic transformations in Ni_2MnGa , as well as the distribution of Ni and Mn atoms within the unit cell. Moreover, the ability of neutrons to distinguish between Ni and Mn allowed to observe the temperature-induced atomic displacements in each sublattice. Cong et al. [40] found that the transformation process in $\text{Ni}_{53}\text{Mn}_{25}\text{Ga}_{22}$ alloys is different from that investigated in stoichiometric Ni_2MnGa alloys, since a pretransformation mechanism seemingly starts in the martensitic phase rather than in the austenitic one. They also demonstrated that the martensitic phase presents a non-modulated tetragonal structure. The same research group [41] analyzed three particular FSMAs ($\text{Ni}_{53}\text{Mn}_{25}\text{Ga}_{22}$, $\text{Ni}_{48}\text{Mn}_{25}\text{Ga}_{22}\text{Co}_5$ and $\text{Ni}_{48}\text{Mn}_{30}\text{Ga}_{22}$) by neutron powder diffraction in order to observe how doping with Co and changing the alloy composition affect the crystal structure at room temperature. The last composition of the three alloys studied presents a cubic austenitic structure at room temperature, whereas the other two present the same martensitic tetragonal structure. They also confirmed that the substitution of Ni for Co does not affect the crystal structure, whereas substituting Ni for Mn does. Orlandi et al. [42,43] investigated the influence of Co doping on the martensitic transformation in stoichiometric Ni_2MnGa . They found that, whereas in Ni_2MnGa and $\text{Ni}_{47}\text{Co}_3\text{Mn}_{25}\text{Ga}_{25}$ the MT takes place in two steps and involves a premartensitic phase, in $\text{Ni}_{45}\text{Co}_5\text{Mn}_{25}\text{Ga}_{25}$ the transition occurs in a single step. They also reported on the presence of long-range antiferromagnetic ordering in the Co-rich Ni-Co-Mn-Ga alloy.

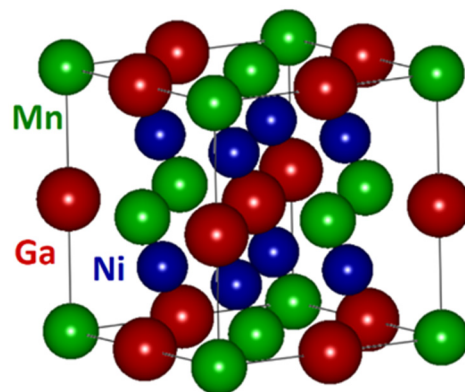


Figure 3. Crystal structure of the Heusler Ni_2MnGa alloy in the austenitic L_{21} cubic phase.

As previously stated, powder neutron diffraction is an excellent tool to analyze atomic ordering. Richard et al. [44] took advantage of this method to study a set of Ga-deficient Ni-Mn-Ga alloys, with excessive Mn and 48–52 at.% Ni. They asserted that, when Ni is presented with a 50 at.%, the Mn in excess occupies Ga sites. When the Ni content is below 50%, Mn in excess tends to occupy Ni and Ga sites, whereas for Ni contents above 50 at.%, excess Ni atoms occupy Mn sites by displacing Mn to Ga sites. As a result of these atomic orderings, Mn atoms at the Ga sites become nearest neighbors to Mn atoms in their proper sites, leading to antiferromagnetic coupling and, hence, to a reduction in the total magnetic moment. These studies were completed by Lázpita et al. [45,46] who recompiled all the data presented by Richard et al. adding a new composition. They studied the martensitic structures and cell parameters of a set of Ga-deficient Ni-Mn-Ga alloys with excess Mn and 43–52 at.% Ni. Samples with excess Ni show a 5M tetragonal martensite structure, while defective Ni alloys present a 7M-modulated orthorhombic structure with a small monoclinic distortion. The nature of the magnetic coupling between Mn atoms at different sites was analyzed in terms of the dependence of the sign of the magnetic exchange integral on the distances between Mn atoms.

Neutron diffraction was used by Wang et al. [47] to disclose the existence of amorphous phases and a MT from tetragonal to cubic phases in the crystallized fraction of $\text{Ni}_{57}\text{Mn}_{27}\text{Ga}_{22}$ nanoparticles prepared by ball-milling and subsequent post-annealing. The amorphous phase in this case was considered to control the transformation kinetics.

Neutron powder diffraction was also employed for the analysis of the atomic site occupancies in more complex doped Ni-Mn-Ga alloys. Roy et al. [48] studied the effect of doping on the properties of Ni_2MnGa . Since Cu tends to occupy Mn sites, Mn atoms are pushed to occupy Ga sites. As a consequence, the Curie temperature (T_C) is lowered and T_M raised, so that, at 25 at.% of Cu the martensitic and magnetic transitions in $\text{Ni}_2\text{Mn}_{0.75}\text{Cu}_{0.25}\text{Ga}$ coincide at 317 K. Pérez-Checa et al. [18] examined by neutrons a set of six Ni-Mn-Ga-Co-Cu-Fe high temperature FSMAs to disclose the influence of Fe doping on the evolution of atoms distribution within the unit cell of the crystal lattice and to correlate the Fe-triggered atomic redistribution with their magnetic properties. They found that the Fe increase provokes an enhancement of the ferromagnetically coupled Mn-Mn pairs at the expense of the antiferromagnetic ones, leading to an increase of the total magnetic moment of the alloy, in agreement with magnetometry measurements on the alloys.

Neutron studies on Ni-Mn-based MetaMSMAs started in the late 2000s. Brown et al. [49] investigated $\text{Ni}_2\text{Mn}_{1.94}\text{Sn}_{0.56}$ by neutron powder diffraction in order to determine the atomic positions within the unit cell and the crystal structure of the martensitic phase. They concluded that Mn atoms in excess occupy vacant Sn sites, and that the martensitic structure is a 4M-modulated orthorhombic one. Mañosa et al. [50] used neutron diffraction to reveal the magnetic field-induced martensitic transformation in the $\text{Ni}_{49.7}\text{Mn}_{34.3}\text{In}_{16.0}$ MetaMSMA, associated with the strong coupling of magnetism and structure. They showed that this coupling led to magnetic superelasticity, magnetic shape memory, giant magnetocaloric and giant inverse magnetocaloric effects. Brown et al. [51] studied a Mn_2NiGa alloy with powder neutron diffraction, revealing that in the parent cubic phase (000) sites are occupied by Mn, (1/2,1/2,1/2) sites by Ga and (1/4,1/4,1/4) and (3/4,3/4,3/4) sites by a mixture of Ni and Mn. Furthermore, from the recorded diffraction patterns at 5 K they deduced that the coupling between Mn atoms in the martensite phase in this alloy is of ferromagnetic nature. Mukadam et al. [52] employed neutron powder diffraction and complementary magnetic characterization techniques in order to study how an increase in Ni and a decrease in Mn contents affect the magnetism in a set of $\text{Ni}_{2+x}\text{Mn}_{1-x}\text{Sn}$ alloys. They concluded that an increase in the Ni content at the expense of Mn atoms produced a reduction of both T_C and the total magnetic moment of the unit cell.

2.1.2. Single Crystal Neutron Diffraction

Single crystal neutron diffraction measures the coherent scattering intensities (Bragg intensities) from a single crystal, so that the crystal structure of the material can be analyzed [53]. The unit cell, space group, positions of the atomic nuclei and site occupancies can be determined with this technique. Since neutrons possess a magnetic moment, the magnetic structure of the material can be determined by analyzing the magnetic contributions to the Bragg peaks. When a single crystal is placed in a beam of neutrons, each set of planes in the sample diffract in certain distinct directions. In order to determine every plane set of the crystalline structure, either an area detector must be employed, or the sample has to be rotated around one crystallographic axis when using a point detector. Figure 4 shows the differences in the diffraction conditions and the signal recording between polycrystalline and single crystal samples. The atomic interplanar spacings can be determined by knowing the measurement angles and employing the Bragg's law [54–57]. For both single crystal and powder neutron diffraction, and by making the corresponding mathematical corrections to the recorded intensity profile at the detector, it is possible to refine the structure and atomic ordering from fittings to that intensity profile using structure refinement programs such as, e.g., Fullprof [58].

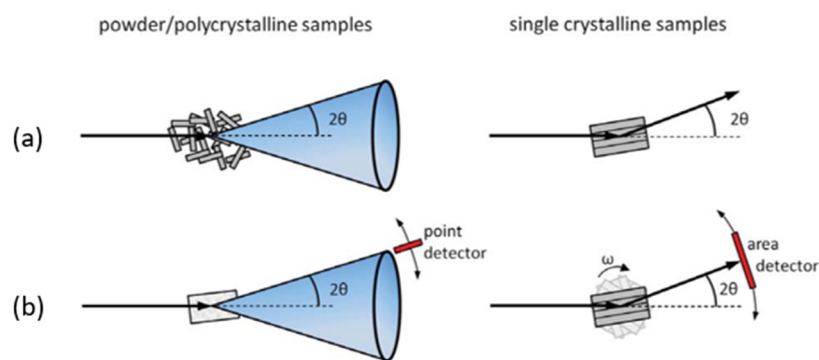


Figure 4. Schematic of sample type (a) and experimental setup (b) for powder/polycrystalline sample (left column) and single crystalline samples (right column). The incoming beam is diffracted taking the shape of a cone both in powder and polycrystalline samples, therefore a point detector being enough to record all the reflections from the sample. Nonetheless, single crystalline samples diffract in specific directions, and the sample must be aligned for each 2θ position of the area detector, being the sample also rotated around its ω axis. Reproduced from Ph.D. Thesis of M. Chmielus, Technische Universität Berlin [55].

Historically, single crystal neutron diffraction has been employed first to determine the structure and atomic positions in ferromagnetic shape memory alloys. Brown et al. [39] carried out single crystal and powder neutron diffraction experiments to establish the diagram of the structural phase transitions in alloy compositions close to the stoichiometric Ni_2MnGa . Glavatsky et al. [59] investigated the effect of alloying on the crystal structure, lattice parameters, MT temperatures and magnetoplasticity of single crystalline $\text{Ni}_{49.4}\text{Mn}_{23.3}\text{Ga}_{25.6}\text{Cu}_{1.7}$, $\text{Ni}_{49.3}\text{Mn}_{27.8}\text{Ga}_{20.9}\text{Cu}_{2.0}$, $\text{Ni}_{47.3}\text{Mn}_{25.5}\text{Ga}_{24.5}\text{Cu}_{2.7}$, $\text{Ni}_{46.8}\text{Mn}_{27.3}\text{Ga}_{22.8}\text{Cu}_{3.1}$ and $\text{Ni}_{49.6}\text{Mn}_{27.6}\text{Ga}_{18.5}\text{Cu}_{3.9}$ FSMAs. Neutron diffraction measurements revealed a change in the structure of the martensitic phase from a 5 M to a 7 M modulated body-centered tetragonal (bct) as a function of the Cu content. Alloying with Cu affected both T_C and T_M due to changes in the valence electron concentrations and in the Mn-Mn and Mn-Ni exchange interactions. Brown et al. [60] examined the crystal structure at different temperatures, the transition temperatures (T_C and T_M) and the MT mechanism under applied stress of a Ni-Fe-Ga FSMA. They found that a cubic-to-tetragonal MT occurs without any orthorhombic intermediate phase in these alloys. Single crystal and powder neutron diffraction techniques were combined by Richard et al. [44] and Lázpita et al. [45,46] to disclose the atomic positions in a set of Ni-Mn-Ga alloys (specific details of their findings are found in the powder neutron diffraction section of the present manuscript). Both types of diffraction in these works confirmed the existence of similar crystal structures of the martensitic phase, as well as similar atomic site occupancies and transition temperatures both in single crystalline and in powder forms.

The transformation behavior of the $\text{Ni}_{50.5}\text{Mn}_{28.2}\text{Ga}_{21.2}$ FSMA single crystal was studied by neutron diffraction in the temperature range of 4–300 K by Glavatsky et al. [61]. They found that an orthorhombic martensitic structure with 5 M modulation remains stable in the 4–300 K temperature range, while the martensite twin mobility suddenly rises at 200 K. Molnar et al. [62] explored by neutron diffraction a stress-induced martensitic variant reorientation in a $\text{Ni}_{49.7}\text{Mn}_{29.3}\text{Ga}_{21}$ single crystal exhibiting a 5 M tetragonal martensite. They demonstrated that the macroscopic strain originates only from the variant redistribution, since no other contributions to that strain were detected. Chmielus et al. [63–65] studied the presence of different martensitic variants in Ni-Mn-Ga FSMAs in comparable ($\text{Ni}_{50.6}\text{Mn}_{28.3}\text{Ga}_{21}$) or distinct ($\text{Ni}_{50.5}\text{Mn}_{28.7}\text{Ga}_{20.8}$) volume fraction alloys. They also determined the lattice parameters and modulation periods in the martensitic phase in these alloys. Kabra et al. [66] studied a Ni_2MnGa alloy by single crystal neutron diffraction to determine the crystallographic orientation relationship between the twinned and untwinned regions. They demonstrated that the orientation relation between both twin variants is a 90° rotation around the b-axis of the original crystal.

2.1.3. Polarized Neutron Diffraction

Neutrons are electrically uncharged but possess a magnetic dipole moment. This moment interacts with the magnetic field of unpaired electrons in the 3d orbitals of the MSMA sample, through either the magnetic field associated with the orbital motion of the electron or the intrinsic dipole moment of the electron itself. As a result, magnetic scattering events occur in addition to the already mentioned structural scattering from the atomic nuclei. When neutrons have their magnetic moments oriented randomly (unpolarized neutron beam) they interact magnetically with the sample and are scattered in all directions, so that the net contribution to the total scattering cross section is usually very low. However, in a polarized neutron beam all the neutron magnetic moments are pointing towards the same direction and the pure magnetic scattering cross section becomes relevant. To polarize and monochromatize the neutron beam, the white unpolarized beam goes through a polarizing single crystal which acts both as monochromator and also as spin filter (see Figure 5). Once the beam is polarized, the neutron beam passes through a spin flipper which modifies the orientation of the polarization, giving rise to neutrons with spins up or down. The analysis of the magnetic moment of the scattered polarized neutrons after hitting the sample allows to obtain a pure magnetic diffraction profile. As a result, the magnetic structure of the sample can be determined. The main difference between the theory of magnetic scattering of neutrons and the theory of nuclear scattering is that magnetic scattering is highly dependent on the direction of the applied magnetic field, leading to a magnetic cross-section with a vector component, whereas the cross-section of nuclear scattering is a scalar quantity [32,33,36,67].

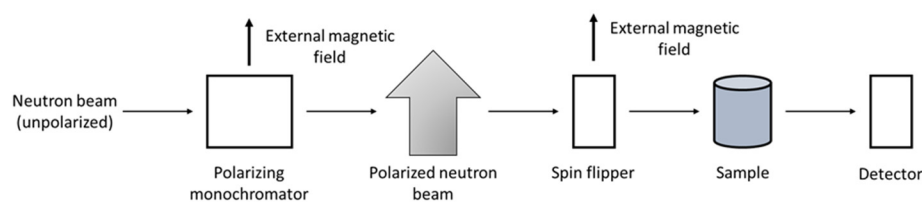


Figure 5. Scheme of a polarized neutron diffraction experimental set-up.

Polarized neutron diffraction is usually employed in single crystal alloys. Since the early 80s, the magnetic structure of Ni-Mn-Ga based FSMAs studied by polarized neutron diffraction has been the focus of several works. Webster et al. [38] employed it to demonstrate that the magnetic moments in the Ni_2MnGa alloy are associated mainly to the Mn sites, with a small contribution from the Ni sites. Brown et al. [68] analyzed the MT in a Ni_2MnGa alloy, observing a magnetic moment transfer from Mn to Ni. This redistribution of electrons between 3d sub-bands of different symmetries led to the conclusion that the cubic-to-tetragonal phase transition is driven by a band Jahn-Teller distortion. Cong et al. [40] complemented neutron powder diffraction studies on $\text{Ni}_{53}\text{Mn}_{25}\text{Ga}_{22}$ by performing polarized neutron diffraction experiments at different temperatures. They concluded that the magnetization becomes weaker as the temperature increases due to the decreasing magnetic ordering, and that there is no intermartensitic transformation in the investigated alloy. Pramanick et al. [69] employed polarized neutron diffraction to establish a correlation between the rotation of magnetic moments and the twin-reorientation phenomena in a $\text{Ni}_2\text{Mn}_{1.14}\text{Ga}_{0.86}$ single crystal. Lázpita et al. [70] performed polarized neutron diffraction measurements to determine the influence of the atomic positions within the crystal unit cell on the magnetic coupling between atoms in the austenitic phase of $\text{Ni}_{51.9}\text{Mn}_{26.2}\text{Ga}_{21.9}$, and in the martensitic phase of $\text{Ni}_{52.6}\text{Mn}_{26.9}\text{Ga}_{20.5}$, the latter presenting a non-modulated tetragonal phase. The analysis of the spin density maps (Figure 6) demonstrates that the main differences between both alloys are the Mn-Mn interatomic distances, which modify the electronic structure and significantly change the total magnetic moment of the alloys. In the austenite phase all the Mn atoms on Ga sites are coupled antiferromagnetically with Mn atoms in their own sites, whereas in the martensitic phase

Mn atoms in these sites couple both ferro- and antiferromagnetically depending on their neighboring atoms. With these results, they demonstrated a crossover of the Mn-Mn coupling, from ferromagnetic to antiferromagnetic, when the Mn-Mn atomic distances change from 3.32 Å to 2.92 Å, respectively.

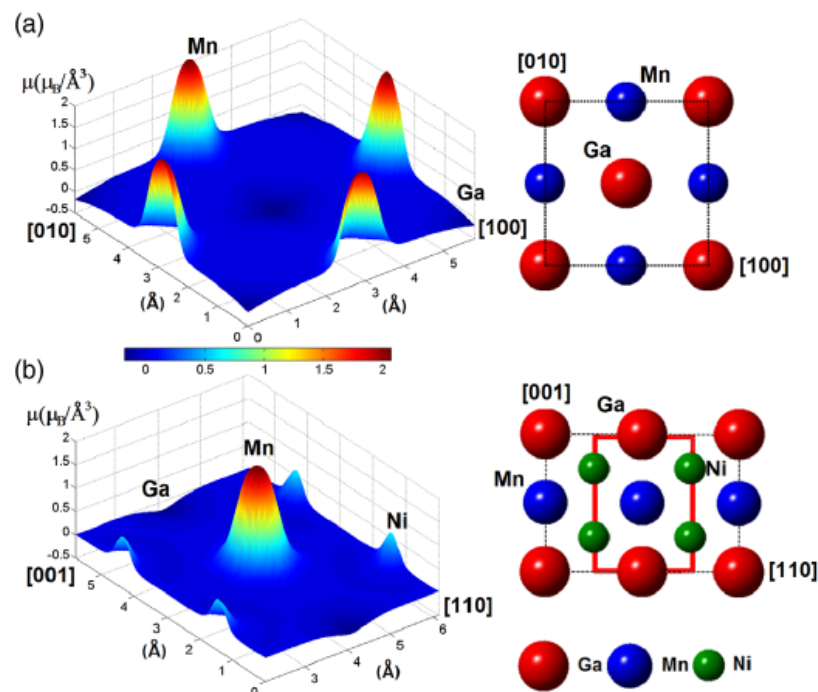


Figure 6. Spin density maps for a $\text{Ni}_{52}\text{Mn}_{26}\text{Ga}_{22}$ FSMA single crystal. These maps were obtained from single crystal polarized neutron diffraction experiments carried out at the D3 instrument (ILL, Grenoble). The maps show the spin density distribution in the (001) plane (a) and in the (-110) plane (b) of the L_{21} structure measured in the ferromagnetic austenite at 330 K under 9 T. Mn and Ni sites show a positive spin density that corresponds to the ferromagnetic coupling of these atoms, while Ga sites present a negative contribution attributed to the antiferromagnetically coupled Mn. The right side of the figure shows the atomic distribution in the aforementioned planes obtained by means of non-polarized single crystal neutron diffraction experiments (D9, ILL). The rectangular red line indicates the fragment of the (-110) plane represented in the corresponding map [70]. Reprinted Figure 4 with permission from P. Lázpita et al., Physical Review Letters 119, 155701 (2017), Copyright (2017) by the American Physical Society.

Neutron diffraction has been extensively used to determine not only the effect of atomic site occupancies on the properties of MSMA, but also the characteristics of the martensitic transformation, being a valuable tool to identify premartensitic phases in these alloys. The criticality of small stoichiometric variations on the MSMA compositions has been identified by several authors, finding that variations as small as 1% in some of the elements forming the MSMA can lead to dramatic changes in the MT temperatures (T_M , T_A), as well as in the magnetic ordering ones (T_C). Moreover, the role of different dopants on the properties of MSMA has been extensive issue of study by means of neutron diffraction. In this way, the effect doping elements have on the crystalline structure of the martensite phases, leading not only to the appearance of crystal structure modulations but also to a change on the crystal lattice space group, has been addressed by many groups studying MSMA. Besides affecting the crystal lattices of MSMA, dopants also have a strong influence on the martensite transformation and magnetic ordering temperatures. Finally, polarized neutron diffraction allows studying the magnetic spin densities in each specific site of the crystal lattices of the MSMA. This opens the door to investigate the magnetic coupling regimes between magnetic elements within the alloy, and changes on the

magnetic properties of the MSMA upon on-purpose stoichiometry modifications and/or the addition of doping elements.

2.2. Large Scale Structures

2.2.1. Small-Angle Neutron Scattering (SANS)

Small-Angle Neutron Scattering (SANS) is a coherent elastic neutron scattering technique largely used for the study of nanoscale inhomogeneities in materials, involving neutron wavelengths typically in the range of tens to hundreds of Angstroms [71]. Since the characteristic sizes studied by SANS are large compared to interatomic distances, the matrix (sample medium) in which these inhomogeneities are embedded is usually treated as continuum and characterized by an average scattering length density. The presence of these inhomogeneities, such as dispersed particles or, as it is the case in MSMA, different crystallographic phases and/or compositions, is detected thanks to the variation of the scattering length density of these nano-inhomogeneities with respect to the medium (homogeneous matrix) [33,36,72,73].

SANS plays an important role in the study of phase-separated MSMA. This is the case of the studies performed by Runov et al. [74,75], who employed Small-Angle Polarized Neutron Scattering (SAPNS) to study a $\text{Ni}_{49.1}\text{Mn}_{29.4}\text{Ga}_{21.5}$ single crystal at different temperatures and under magnetic fields. They found an asymmetry in the polarized neutron scattering intensity profiles at around 150 K, which led them to determine the coexistence of two different phase transformations: the martensitic phase transformation expected at 306 K and an unexpected one at 150 K. The different magnetic orderings present in each phase are responsible for the change in polarization observed with SAPNS. Using standard (non-polarized) SANS, an interesting work has been performed by Sun et al. [76,77], who analyzed the decomposition of a face centered cubic (fcc) martensite phase in $\text{Mn}_{19}\text{Cu}_2\text{Al}_4\text{Ni}$, accompanied by the formation of Cu-rich clusters and an α -Mn phase under different ageing treatments. They observed fewer and larger clusters when higher temperature and longer time ageing processes were used. They also determined that the martensitic phase decomposition is a process characterized by a two-step linear kinetic regime: the first one with a larger slope was observed for aging times below 16 h, and the second one with a smaller slope for aging times larger than 16 h. The presence of ferromagnetic nanoprecipitates in an antiferromagnetic matrix was reported by Benacchio et al. [78] in a bulk $\text{Ni}_{50}\text{Mn}_{45}\text{In}_5$ MetaMSMA field-annealed at 700 K. The results were obtained by combining unpolarized and spin-polarized SANS. This phenomenon was also studied by Sarkar et al. [79], who demonstrated the presence of spin-clusters of structural origin in a $\text{Ni}_{45}\text{Co}_5\text{Mn}_{38}\text{Sn}_{12}$ MetaMSMA, which are related to the martensitic transformation. Kopitsa et al. [80] and Bliznuk et al. [81] studied the nuclear and magnetic structures in FeMn-based alloys doped with Si, Cr or Ni, affected by interstitial C and N atoms. Fe-Mn, Fe-Mn-Si, Fe-Mn-Si-Cr, Fe-Mn-Si-Cr-Ni solid solutions were analyzed, revealing that Si enhances the chemical homogeneity of the studied alloys, N does not influence substantially their homogeneity and C worsens it.

2.2.2. Reflectometry

This technique is used in MSMA thin films, commonly in combination with XRD and neutron diffraction techniques, and consists in the study of the characteristics of a neutron beam reflected from the sample. The intensity profile of the reflected beam is recorded as a function of the incident and reflected angles, or of the neutron wavelengths. The shape of the reflectivity profile yields information about the thickness, density and roughness of any thin film (with thickness from several nm to several hundreds of nm) layered onto the substrate [82]. The presence of periodic maxima and minima in the intensity profile determines the thickness of the layer or layers composing the sample, being the number of superimposed maxima and minima directly related with the number of layers present in the film. The surface roughness of the film is determined by the shape of the intensity curve, which falls faster for rougher samples. The one-dimensional scattering length density (SLD)

profile of the sample along its surface normal, with nanometer resolution, is derived from the analysis of the reflectometry data. The main advantage of this technique lies in the possibility of studying textures and interplanar distances, alongside with the fact that neutron reflectometry can differentiate if layers are made of different metals [83].

If the neutron beam is polarized, it is possible to record polarized neutron reflectometry curves that give information about the magnetic depth profile of the sample being investigated. Normally four reflectivity curves are obtained during experiments with polarized neutrons. Spin-flip ($R+ -$ and $R- +$; changes in the polarization of the neutrons after reflection) and non-spin-flip ($R+ +$ and $R- -$; neutrons that keep the initial polarization after reflection) reflectivity processes are usually analyzed. The “+” is used when the spins of the neutrons are parallel to the applied external magnetic field, the “-” is used when the spins are antiparallel to the field. It should be mentioned that in-plane magnetization components which are not parallel to an external magnetic field contribute to spin-flip process (spin-down neutron will be reflected as a spin-up neutron ($R- +$) and vice-versa). The difference of $R+ +$ and $R- -$ clearly indicates the presence of an in-plane magnetic moment (magnetic SLD components) collinear to the external field. In this way, reflectometry allows to determine how magnetic domains are distributed through the depth of the thin film. Hence, polarized neutron reflectometry is a very versatile technique to study surfaces, interfaces and layer compositions in multi-layered thin films, both structurally and magnetically [84–86]. Even if this is not an outstanding technique for the study of bulk and powder MSMA, it can provide useful information about MSMA thin films. Granovsky et al. [87] performed polarized neutron reflectometry measurements to analyze the induced magnetic moment in a 25 nm-thick $\text{Ni}_{50}\text{Mn}_{35}\text{In}_{15}$ thin film. Under an applied magnetic field of 5 kOe, results show no detectable in-plane magnetization at room temperature, while an induced magnetic moment collinear with the applied magnetic field is present at low temperatures.

Although not as extensively as neutron diffraction, small angle neutron scattering and neutron reflectometry have also been employed to investigate MSMA by using polarized neutron beams. In particular polarized SANS has been employed to investigate the magnetic orderings of martensite phases in MSMA, as well as the presence of magnetic spin clusters in these alloys upon doping and/or the use of interstitial light elements to enhance the MSMA properties. Polarized neutron reflectometry has been employed to investigate the magnetic depth profile of MSMA thin films with and without the presence of an external magnetic field.

2.3. Neutron Imaging

2.3.1. Texture Diffractometry

Texture diffractometry measurements are used to determine the orientation distribution of crystalline grains within a polycrystalline sample. A material is considered to be textured if the grains are crystallographically aligned along a preferred direction. This neutron imaging method for texture analysis is based on neutron diffraction, similarly to its analogue X-ray diffraction (XRD) technique [88]. Texture diffractometry measurements give as a result images with the textures present in the material. As already mentioned, the main advantage of neutron diffraction over X-ray diffraction arises from the fact that the interaction of neutrons with the material is relatively weak and it is not related to the number of protons (Z) of the elements composing the sample, and that the penetration depth of neutrons is much larger than the one of X-rays [89–91]. The application of this technique offers distinct advantages in texture determinations, particularly for samples with low angle reflections where intensity corrections for X-rays are most critical. As previously discussed in other neutron scattering techniques, it is possible to measure magnetic scattering events that give, as a result, magnetic texture analysis. This is particularly interesting for crystals with an antiferromagnetic component, where peaks exist in the diffraction pattern which are due solely to the magnetic scattering [89–91].

Neutron diffractometry imaging has been used for texture analysis in polycrystalline Ni-Mn-Ga FSMA by several authors. Cong et al. [41], alongside with powder

diffraction studies, performed texture measurements in $\text{Ni}_{53}\text{Mn}_{25}\text{Ga}_{22}$ and Co-doped $\text{Ni}_{48}\text{Mn}_{25}\text{Ga}_{22}\text{Co}_5$ alloys, concluding that the presence of strong textures is due to the hot-forging processing of the alloys. Several texture changes caused by the rearrangement of martensitic variants were observed in the Co-doped alloy during deformation, concluding as a consequence that changes in texture are closely related to the shape memory effect. The changes in texture on $\text{Ni}_{48}\text{Mn}_{30}\text{Ga}_{22}$ and $\text{Ni}_{53}\text{Mn}_{25}\text{Ga}_{22}$ FSMA were studied by Nie et al. [92], who observed that after a compression stress was imposed on the parent phase, a strong preferred selection of two martensitic twin variants was observed in the obtained martensitic phase. Chulist et al. [93] studied the impact of the fabrication process on the texture presence in the alloys, analyzing two polycrystalline samples fabricated by directional solidification ($\text{Ni}_{50}\text{Mn}_{29}\text{Ga}_{21}$) and hot rolling ($\text{Ni}_{50}\text{Mn}_{30}\text{Ga}_{20}$). The solidified alloy is characterized by $\langle 100 \rangle$ fiber textures along the growth direction, while the hot rolling processing gave rise to a weak $\{111\} \langle 112 \rangle$ recrystallization texture in the alloy.

2.3.2. Radiography/Tomography

In radiographic methods, the attenuation of an incident neutron beam on passing through an object is used to study the internal structure (at micrometer length scale) of this object without destroying it. By using this radiography technique, 2D images of the sample being investigated are obtained, while by using tomography techniques, 3D images are obtained. Neutron radiography and tomography techniques are preferable over equivalent X-Rays techniques due to the high penetration depth of neutrons, which allows large samples to be investigated. Moreover, light elements can be detected in an environment dominated by heavy elements, as occurs in every neutron technique. Among the advantages of these methods, the possibility of obtaining maps of grain shapes and crystallographic orientations are noteworthy [94,95].

Kabra et al. [66] complemented single crystal neutron diffraction studies with energy dispersed neutron imaging, yielding as a result the morphology of the twinned regions in a stoichiometric Ni_2MnGa alloy. They found that this single crystal can spontaneously twin upon the application of an external field, showing the orientation relation between the untwinned and twinned regions, together with their specific morphology and the mosaic microstructure of the original crystal. Samothrakitis et al. [96] investigated the 3D microstructure of a hot-extruded $\text{Co}_{49}\text{Ni}_{21}\text{Ga}_{30}$ FSMA by neutron diffraction tomography. They found that no preferred crystallographic orientations can be appreciated in the nearly spherical grains observed in the sample.

The use of neutron imaging techniques in MSMA has helped understanding the origin of the presence of textures in these alloys, attributing it to either the presence of doping elements, off-stoichiometric compositions or the alloy casting technique employed.

3. Inelastic Neutron Scattering Studies of MSMA

Inelastic neutron scattering (INS) techniques are usually employed with the aim of studying the disorder in the crystalline structure of MSMA, either positional or substitutional [97]. Due to this disorder, the intensity of the typically obtained Bragg spots within a neutron diffraction technique is reduced, as a consequence of the fact that the whole crystal does not contribute coherently to the diffraction spots due to lattice imperfections. Otherwise, in a perfect sample with a completely uniform crystal lattices the diffuse scattering (which is of inelastic nature) would be zero, and the Bragg spots would be sharp. Nonetheless, the positions of the Bragg spots are not affected. The intensity changes due to diffuse scattering events are redistributed along the diffractogram. The distribution of these intensity changes may be either uniform across the whole reciprocal lattice or concentrated in a particular anisotropic direction according to the nature of disorder correlations between neighboring cells. This diffuse scattering, thus, arises from the local configuration of the material: it is a short-range effect, while the long-range structural order does not contribute to it [33,36,98,99].

As stated in the introduction to this review, diffuse scattering is not widely used for this kind of alloys. Nevertheless, there are a few cases where this technique has been employed to study phonon dispersion in MSMA. Zheludev et al. [100,101] studied the phonon spectra in a Ni_2MnGa single crystal in a wide temperature range above 220 K, which corresponds to the temperatures of stability of the cubic phase. An incomplete, but strong, softening at wave vector $\xi_0 \approx 0.33$ in the $[\xi, \xi, 0]$ TA_2 phonon branch was observed both above and below T_C of the austenite phase. During cooling, the frequency of this ξ_0 soft mode was strongly reduced down to zero at about $T_I = 250$ K which resulted from a premartensitic first-order phase transition from austenite into a soft-mode condensed intermediate phase. The origin of the phonon anomaly was attributed to the electron-phonon interactions. Similar inelastic neutron scattering measurements were performed in Ni_2MnGa by Recarte et al. [102], who investigated the influence of the magnetic field on the TA_2 -phonon branch in the temperature range where the aforementioned intermediate transition takes place. As a result, a strong enhancement of the magnetoelastic interactions at the intermediate transition and the significant role of the magnetism in the phonon dispersion events were revealed.

Even when most neutron diffuse scattering experiments were focused on Ni-Mn-Ga alloys, other NiMn-based alloys were also investigated by this technique. Zheludev et al. [101] and Moya et al. [103,104] concluded that the results of the diffuse polarized neutron scattering carried out in several experiments in Ni-Mn-Ga, Ni-Mn-Sn, Ni-Mn-Sb, Ni-Mn-Al and Ni-Mn-In (Figure 7) alloys demonstrate unequivocally that, similarly to what occurs in body-centered cubic (bcc) alloys, acoustic phonons in the transverse TA_2 branch possess energies significantly lower than those in the other branches. Furthermore, they also demonstrated that phonons along other symmetry directions also possess energies larger than those of the TA_2 branch.

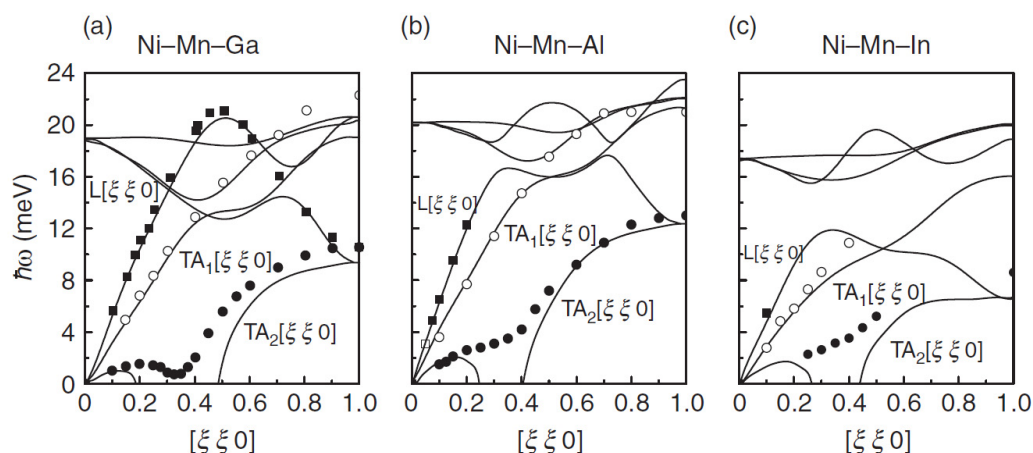


Figure 7. Phonon dispersion curves along the $[\xi, \xi, 0]$ direction for Ni_2MnGa (a), $\text{Ni}_{54}\text{Mn}_{23}\text{Al}_{23}$ (b) and $\text{Ni}_{49.3}\text{Mn}_{34.2}\text{In}_{16.5}$ (c). Symbols correspond to inelastic neutron scattering data (diffuse scattering) at temperatures well above the martensitic transition; lines correspond to the ab-initio calculations of the phonon dispersion curves along the experimentally determined directions in the stoichiometric Ni_2MnZ [2]. Reprinted from Handbook of Magnetic Materials, 19C, M.Acet, Ll.Mañosa and A.Planes, Magnetic-Field-Induced Effects in Martensitic Heusler-Based Magnetic Shape Memory Alloys, 231–289, Copyright (2011), with permission from Elsevier.

Inelastic neutron scattering experiments on MSMA reveal the changes on their phonon dispersion curves when the alloys suffer from either a structural or a magnetic phase transition. This allows to identify unambiguously the phonon dispersion curves with the specific structural and magnetic phases present in the alloys. Furthermore, INS experiments in MSMA with different compositions yield specific phonon dispersion curves for each alloy, being therefore these curves specific fingerprints of the alloy being investigated.

4. Summary

The use of neutron-based techniques to complement basic characterization methods commonly employed in the field of MSMAs is of great interest to the scientific community working in this class of materials. The well-established strong interdependence between the main properties of the alloys (martensitic transformation temperatures, maximum deformation, magnetic transition temperatures, etc.) and their crystal lattices and atomic site occupancies makes the use of neutron diffraction a crucial technique to study MSMAs. A huge number of powder and single crystal neutron diffraction experiments have been performed by scientists from everywhere around the globe, yielding with outstanding precision not only the crystalline phases of the alloys, together with their modulations and phase coexistences when relevant, but also the precise atomic site occupancies and magnetic site densities of alloys made of up to six elements. Doping stoichiometric Ni_2MnGa with different elements, the effect of different alloy casting techniques with similar compositions on the alloy performances, or the relevance of Mn-Mn interactions within the magnetic behavior of the alloys are a few examples where neutron diffraction techniques excel.

Small angle neutron scattering and neutron reflectometry experiments, although less numerous than the aforementioned diffraction ones, have also been conducted in MSMAs of different nature. Small angle neutron scattering has been mainly employed to determine phase segregations, both structural and magnetic, as well as to study the presence of certain element-specific rich regions within the MSMAs. Neutron reflectometry has been utilized to investigate the magnetic depth profile of MSMA thin films, being this technique of great potential interest to investigate the interface quality and associated residual stresses in coupled MSMA thin films.

Neutron imaging, and in particular texture diffractometry and radiography (2D) and tomography (3D), provide information about the presence of textures and their preferred orientations, as well as about the in-plane and 3D morphology of twinned regions within the martensitic phases of MSMAs.

In addition to the elastic neutron scattering techniques summarized above, inelastic neutron scattering, namely diffuse scattering experiments, have been performed in MSMAs. These experiments yield valuable information about the phonon dispersion curves for the studied MSMAs, with particular attention to the changes in dispersion events taking place across the phase transformations. All the neutron scattering experiments on MSMAs discussed in the present manuscript have been listed in Table A1, which is presented in Appendix A.

Neutron sources worldwide are continuously being employed to investigate MSMAs, including ILL (Grenoble, France), ISIS (Oxfordshire, UK), FRM-2 (Munich, Germany), NIST (Maryland, USA), SNS (Oak Ridge, USA) and ANSTO (Sydney, Australia).

The use of neutron scattering techniques to study MSMAs suppose great advances in the basic and applied knowledge of the behavior and properties of these interesting alloys. With a future in which the next-generation neutron sources, with improved brilliance, flux and polarization capabilities of their neutron beams, will complement the already existing ones and increase the availability of neutron beams, the interest and relevance of the neutron studies will continue its rise and popularity around the MSMA community.

Author Contributions: Conceptualization, J.M.P.; methodology, N.A.R.-L. and P.L.; writing—original draft preparation, N.A.R.-L. and J.M.P.; writing—review and editing, all authors; supervision, V.C. and J.M.P. All authors have read and agreed to the published version of the manuscript.

Funding: This work has been carried out with the financial support of the Spanish Ministry of Science, Innovation and Universities (project RTI2018-094683-B-C53-54) and Basque Government Department of Education (project IT1245-19). N.A.R.-L. wants to thank the Basque Government (Department of Education) for providing funding under the specific investigation PFPI grant.

Conflicts of Interest: The authors declare no conflict of interest.

Appendix A

Table listing the literature discussed throughout the manuscript, including references, compositions of the alloys studied, first authors, neutron scattering technique employed and an express summary of the investigation carried out in each publication.

Table A1. List of the literature discussed throughout the present review manuscript. PND: powder neutron diffraction; SCND: single crystal neutron diffraction; SANS: small angle neutron scattering; NR: neutron reflectometry; INS: inelastic neutron scattering.

Ref	Composition	First Author	Technique	Express Summary
[18]	NiMnGaCoCuFe	Pérez-Checa	PND	Effect of Fe doping on atomic ordering and magnetic properties
[39]	Ni ₂ MnGa	Brown	PND	MT phase diagram determination
[40]	NiMnGa	Cong	Polarized PND	Differences in the MT in stoichiometric and non-stoichiometric NiMnGa
[41]	NiMnGaCo	Cong	PND, Imaging	Effect of Co doping on crystal structure
[42]	NiMnGaCo	Orlandi	PND	Effect of Co doping on MT
[43]	NiMnGaCo	Orlandi	PND	Effect of Co doping on MT
[44]	NiMnGa	Richard	PND, SCND	Ni and Mn content effect on atomic ordering
[45]	NiMnGa	Lázpita	PND, SCND	Ni and Mn content effect on atomic ordering
[46]	NiMnGa	Lázpita	PND	Ni and Mn content effect on atomic ordering
[47]	NiMnGa	Wang	PND	Study of amorphous phases and MT
[48]	NiMnGaCu	Roy	PND	Effect of Cu doping on TC and TM
[49]	NiMnSn	Brown	PND	Study of atomic ordering and crystal unit cell
[50]	NiMnIn	Mañosa	PND	Study of the magnetic field-induced MT
[51]	Mn ₂ NiGa	Brown	PND	Study of atomic ordering and crystal unit cell
[52]	NiMnSn	Mukadam	PND	Ni and Mn content effect on magnetism
[59]	NiMnGaCu	Glavatskyy	SCND	Cu doping effect on crystal structures, MT and magnetoplasticity
[60]	NiFeGa	Brown	SCND	Effect of applied stress on TC, TM and MT mechanism
[61]	NiMnGa	Glavatskyy	SCND	Study of the MT behavior
[62]	NiMnGa	Molnar	SCND	Study of the stress-induced martensitic variants reorientation
[63]	NiMnGa	Chmielus	SCND	Study of lattice parameters and modulations
[64]	NiMnGa	Chmielus	SCND	Study of lattice parameters and modulations
[65]	NiMnGa	Chmielus	SCND	Study of lattice parameters and modulations
[66]	Ni ₂ MnGa	Kabra	SCND, Imaging	Study of the crystallographic orientation relationship in twinned/untwinned regions
[38]	Ni ₂ MnGa	Webster	Polarized PND	Magnetic site densities in Ni and Mn sites
[68]	Ni ₂ MnGa	Brown	Polarized SCND	Ni to Mn magnetic moment transfer in MT
[69]	NiMnGa	Pramanick	Polarized SCND	Correlation between twin-reorientation and rotation of magnetic moments

Table A1. Cont.

Ref	Composition	First Author	Technique	Express Summary
[70]	NiMnGa	Lázpita	Polarized SCND	Influence of atomic ordering on magnetic coupling between Mn atoms
[74]	NiMnGa	Runov	SANS	Evidence for an intramartensitic phase transition
[75]	NiMnGa	Runov	SANS	Study of spin-spin correlation radius upon cooling to TM
[76]	NiMnCuAl	Sun	SANS	Effect of ageing treatments on Cu- and Mn-rich cluster formation
[77]	NiMnCuAl	Sun	SANS	Effect of ageing treatments on Cu- and Mn-rich cluster formation
[78]	NiMnIn	Benacchio	SANS	Presence of ferromagnetic nanoprecipitates in an antiferromagnetic background
[79]	NiMnCoSn	Sarkar	SANS	Presence of spin-clusters related to MT
[80]	FeMn, FeMnSi, FeMnSiCr, FeMnSiCrNi	Kopitsa	SANS	Effect of Si, Cr and Ni doping and interstitial C and N atoms on MSMA homogeneity
[81]	FeMn, FeMnSi, FeMnSiCr, FeMnSiCrNi	Bliznuk	SANS	Effect of Si, Cr and Ni doping and interstitial C and N atoms on MSMA homogeneity
[87]	NiMnIn	Granovsky	NR	Analysis of induced magnetic moment collinear with the applied field at low T
[92]	NiMnGa	Nie	Imaging	Effect of applied stress on twin variants
[93]	NiMnGa	Chulist	Imaging	Alloy casting method effect on crystal textures
[96]	CoNiGa	Samothrakitis	Imaging	3D microstructure and crystal orientation
[100]	Ni ₂ MnGa	Zheludev	INS	Determination of phonon dispersion curves
[101]	Ni ₂ MnGa	Zheludev	INS	Determination of phonon dispersion curves
[102]	Ni ₂ MnGa	Recarte	INS	Influence of magnetic field on phonon dispersion curves
[103]	NiMnIn	Moya	INS	Determination of phonon dispersion curves
[104]	NiMnX (X = Ga, In, Sn, Sb, Al)	Moya	INS	Determination of phonon dispersion curves

References

- Heczko, O.; Scheerbaum, N.; Gutfleisch, O. Magnetic shape memory phenomena. *Nanoscale Magn. Mater. Appl.* **2009**, 399–439. [\[CrossRef\]](#)
- Acet, M.; Mañosa, L.; Planes, A. Magnetic-Field-Induced Effects in Martensitic Heusler-Based Magnetic Shape Memory Alloys. *Handb. Magn. Mater.* **2011**, 19, 231–289.
- L'vov, V.A.; Chernenko, V.A.; Barandiaran, J.M. Magnetic shape memory materials with improved functional properties: Scientific aspects. In *Novel Functional Magnetic Materials*; Springer International Publishing: Berlin/Heidelberg, Germany, 2016; Volume 231, pp. 1–40.
- Chernenko, V. Magnetostrictive Ni-Mn-Based Heusler Alloys. *Ref. Modul. Mater. Sci. Mater. Eng.* **2021**. [\[CrossRef\]](#)
- Karaca, H.E.; Karaman, I.; Basaran, B.; Ren, Y.; Chumlyakov, Y.I.; Maier, H. J Magnetic field-induced phase transformation in NiMnCoIn magnetic shape-memory alloys—a new actuation mechanism with large work output. *Adv. Funct. Mater.* **2009**, 19, 983–998. [\[CrossRef\]](#)
- Faran, E.; Shilo, D. Ferromagnetic Shape Memory Alloys—Challenges, Applications, and Experimental Characterization. *Exp. Tech.* **2016**, 40, 1005–1031. [\[CrossRef\]](#)
- Billinge, S.J.L.; Levin, I. The problem with determining atomic structure at the nanoscale. *Science* **2007**, 316, 561–565. [\[CrossRef\]](#)
- Ping Liu, J.; Gutfleisch, O.; Fullerton, E.; Sellmyer, D.J. Nanoscale magnetic materials and applications. *Nanoscale Magn. Mater. Appl.* **2009**. [\[CrossRef\]](#)

9. Isnard, O. A review of in situ and/or time resolved neutron scattering. *Comptes Rendus Phys.* **2007**, *8*, 789–805. [[CrossRef](#)]
10. Otsuka, K.; Wayman, C.M. *Shape Memory Materials*. Unitex; Cambridge University Press: Cambridge, UK, 1999.
11. Chowdhury, P.; Sehitoglu, H. Deformation physics of shape memory alloys—Fundamentals at atomistic frontier. *Prog. Mater. Sci.* **2017**, *88*, 49–88. [[CrossRef](#)]
12. Petrini, L.; Migliavacca, F. Biomedical Applications of Shape Memory Alloys. *J. Metall.* **2011**, *2011*, 1–15. [[CrossRef](#)]
13. Kohl, M. *Shape Memory Microactuators*; Springer Science & Business Media: Berlin/Heidelberg, Germany, 2004.
14. Murray, S.J.; Marioni, M.; Allen, S.M.; O’Handley, R.C.; Lograsso, T.A. 6% magnetic-field-induced strain by twin-boundary motion in ferromagnetic Ni-Mn-Ga. *Appl. Phys. Lett.* **2000**, *77*, 886–888. [[CrossRef](#)]
15. Chernenko, V.A.; L’vov, V.A.; Cesari, E.; Barandiaran, J.M. Fundamentals of magnetocaloric effect in magnetic shape memory alloys. In *Handbook of Magnetic Materials*; Elsevier: Amsterdam, The Netherlands, 2019; Volume 28, pp. 1–45.
16. Straka, L.; Heczko, O.; Seiner, H.; Lanska, N.; Drahoukoupil, J.; Soroka, A.; Fähler, S.; Hänninen, H.; Sozinov, A. Highly mobile twinned interface in 10 M modulated Ni-Mn-Ga martensite: Analysis beyond the tetragonal approximation of lattice. *Acta Mater.* **2011**, *59*, 7450–7463. [[CrossRef](#)]
17. Checa, A.P. Development of New Ni-Mn-Ga based High Temperature Shape Memory Alloys. Ph.D. Thesis, University of the Basque Country, Biscay, Spain, 2019.
18. Pérez-Checa, A.; Porro, J.M.; Feuchtwanger, J.; Lázpita, P.; Hansen, T.C.; Mondelli, C.; Sozinov, A.; Barandiarán, J.M.; Ullakko, K.; Chernenko, V. Role of Fe addition in Ni-Mn-Ga-Co-Cu-Fe ferromagnetic shape memory alloys for high-temperature magnetic actuation. *Acta Mater.* **2020**, *196*, 549–555. [[CrossRef](#)]
19. Ito, W.; Imano, Y.; Kainuma, R.; Sutou, Y.; Oikawa, K.; Ishida, K. Martensitic and magnetic transformation behaviors in Heusler-type NiMnIn and NiCoMnIn metamagnetic shape memory alloys. *Metall. Mater. Trans. A Phys. Metall. Mater. Sci.* **2007**, *38*, 759–766. [[CrossRef](#)]
20. Umetsu, R.Y.; Xu, X.; Kainuma, R. NiMn-based metamagnetic shape memory alloys. *Scr. Mater.* **2016**, *116*, 1–6. [[CrossRef](#)]
21. Kainuma, R.; Imano, Y.; Ito, W.; Sutou, Y.; Morito, H.; Okamoto, S.; Kitakami, O.; Oikawa, K.; Fujita, A.; Kanomata, T.; et al. Magnetic-field-induced shape recovery by reverse phase transformation. *Nature* **2006**, *439*, 957–960. [[CrossRef](#)] [[PubMed](#)]
22. Krenke, T.; Duman, E.; Acet, M.; Wassermann, E.F.; Moya, X.; Manosa, L.; Planes, A. Inverse magnetocaloric effect in ferromagnetic Ni-Mn-Sn alloys. *Nat. Mater.* **2005**, *4*, 450–454. [[CrossRef](#)]
23. Dunand, D.C.; Müllner, P. Size effects on magnetic actuation in Ni-Mn-Ga shape-memory alloys. *Adv. Mater.* **2011**, *23*, 216–232. [[CrossRef](#)]
24. Wang, J.; Jiang, C.; Techapiesanchaenokij, R.; Bono, D.; Allen, S.M.; O’Handley, R.C. Microstructure and magnetic properties of melt spinning Ni-Mn-Ga. *Intermetallics* **2013**, *32*, 151–155. [[CrossRef](#)]
25. Jones, H. Chapter 3 Rapid solidification. *Pergamon Mater. Ser.* **1999**, *2*, 23–45.
26. Chernenko, V.A.; Kokorin, V.V.; Vitenko, I.N. Properties of ribbon made from shape memory alloy Ni₂MnGa by quenching from the liquid state. *Smart Mater. Struct.* **1994**, *3*, 80–82. [[CrossRef](#)]
27. Gaitzsch, U.; Pötschke, M.; Roth, S.; Rellinghaus, B.; Schultz, L. A 1% magnetostrain in polycrystalline 5M Ni-Mn-Ga. *Acta Mater.* **2009**, *57*, 365–370. [[CrossRef](#)]
28. Aseguinolaza, I.R.; Orue, I.; Svalov, A.V.; Wilson, K.; Müllner, P.; Barandiarán, J.M.; Chernenko, V.A. Martensitic transformation in Ni-Mn-Ga/Si(100) thin films. *Thin Solid Film* **2014**, *558*, 449–454. [[CrossRef](#)]
29. Lambrecht, F.; Lay, C.; Aseguinolaza, I.R.; Chernenko, V.; Kohl, M. NiMnGa/Si Shape Memory Bimorph Nanoactuation. *Shape Mem. Superelasticity* **2016**, *2*, 347–359. [[CrossRef](#)]
30. Bailey, I.F. A review of sample environments in neutron scattering. *Z. Fur Krist.* **2003**, *218*, 84–95. [[CrossRef](#)]
31. Sears, V.F. Neutron scattering lengths and cross sections. *Neutron News* **1992**, *3*, 26–37. [[CrossRef](#)]
32. Pynn, R. *Neutron Scattering Primer*; Los Alamos Science: Los Alamos, NM, USA, 1990; Volume 19.
33. Willis, B.T.M.; Carlile, C.J. Experimental Neutron Scattering. *Anim. Genet.* **2009**, *39*, 561–563.
34. Orench, I.P.; Clergeau, J.F.; Martínez, S.; Olmos, M.; Fabelo, O.; Campo, J. The new powder diffractometer D1B of the Institut Laue Langevin. *J. Phys. Conf. Ser.* **2014**, *549*, 12003. [[CrossRef](#)]
35. Aubert, A.; Puente-Orench, I.; Porro, J.M.; Luca, S.; Garitaonandia, J.S.; Barandiaran, J.M.; Hadjipanayis, G.C. Denitrogenation process in ThMn₁₂ nitride by *in situ* neutron powder diffraction. *Phys. Rev. Mat.* **2021**, *5*, 014415.
36. Baruchel, J.; Hodeau, J.L.; Lehmann, M.S.; Regnard, J.R.; Schlenker, C. *Neutron and Synchrotron Radiation for Condensed Matter Studies*. *Neutron and Synchrotron Radiation for Condensed Matter Studies*; EDP Sciences; Springer: Berlin/Heidelberg, Germany, 1994. [[CrossRef](#)]
37. Albinati, A.; Willis, B.T.M. The Rietveld method in neutron and X-ray powder diffraction. *J. Appl. Crystallogr.* **1982**, *15*, 361–374. [[CrossRef](#)]
38. Webster, P.J.; Ziebeck, K.R.A.; Town, S.L.; Peak, M.S. Magnetic order and phase transformation in Ni₂MnGa. *Philos. Mag. B* **1984**, *49*, 295–310. [[CrossRef](#)]
39. Brown, P.J.; Crangle, J.; Kanomata, T.; Matsumoto, M.; Neumann, K.-U.; Ouladdiaf, B.; Ziebeck, K. The crystal structure and phase transitions of the magnetic shape memory compound Ni₂MnGa. *J. Phys. Condens. Matter.* **2002**, *14*, 10159–10171. [[CrossRef](#)]
40. Cong, D.Y.; Zetterström, P.; Wang, Y.D.; Delaplane, R.; Peng, R.L.; Zhao, X.; Zuo, L. Crystal structure and phase transformation in Ni₅₃Mn₂₅Ga₂₂ shape memory alloy from 20 K to 473 K. *Appl. Phys. Lett.* **2005**, *87*, 85–88. [[CrossRef](#)]

41. Cong, D.Y.; Wang, Y.D.; Lin Peng, R.; Zetterström, P.; Zhao, X.; Liaw, P.K.; Zuo, L. Crystal structures and textures in the hot-forged Ni-Mn-Ga shape memory alloys. *Metall. Mater. Trans. A Phys. Metall. Mater. Sci.* **2006**, *37*, 1397–1403. [[CrossRef](#)]
42. Orlandi, F.; Çakır, A.; Manuel, P.; Khalyavin, D.D.; Acet, M.; Righi, L. Neutron diffraction and symmetry analysis of the martensitic transformation in Co-doped Ni₂MnGa. *Phys. Rev. B* **2020**, *101*, 1–13. [[CrossRef](#)]
43. Orlandi, F.; Fabbri, S.; Albertini, F.; Manuel, P.; Khalyavin, D.D.; Righi, L. Long-range antiferromagnetic interactions in Ni-Co-Mn-Ga metamagnetic Heusler alloys: A two-step ordering studied by neutron diffraction. *Phys. Rev. B* **2016**, *94*, 1–5. [[CrossRef](#)]
44. Richard, M.L.; Feuchtwanger, J.; Allen, S.M.; O’Handley, R.C.; Lázpita, P.; Barandiarán, J.M.; Gutierrez, J.; Ouladdiaf, B.; Mondelli, C.; Lograsso, T.; et al. Chemical order in off-stoichiometric Ni-Mn-Ga ferromagnetic shape-memory alloys studied with neutron diffraction. *Philos. Mag.* **2007**, *87*, 3437–3447. [[CrossRef](#)]
45. Lázpita, P.; Barandiarán, J.M.; Gutiérrez, J.; Richard, M.; Allen, S.M.; O’Handley, R.C. Magnetic and structural properties of non-stoichiometric Ni-Mn-Ga ferromagnetic shape memory alloys. *Eur. Phys. J. Spec. Top.* **2008**, *158*, 149–154. [[CrossRef](#)]
46. Lázpita, P.; Barandiarán, J.M.; Gutiérrez, J.; Feuchtwanger, J.; Chernenko, V.A.; Richard, M.L. Magnetic moment and chemical order in off-stoichiometric Ni-Mn-Ga ferromagnetic shape memory alloys. *New J. Phys.* **2011**, *13*, 033039. [[CrossRef](#)]
47. Wang, Y.D.; Ren, Y.; Nie, Z.H.; Liu, D.M.; Zuo, L.; Choo, H.; Li, H.; Liaw, P.K.; Yan, J.Q.; McQueeney, R.J.; et al. Structural transition of ferromagnetic Ni₂MnGa nanoparticles. *J. Appl. Phys.* **2007**, *101*, 1–7. [[CrossRef](#)]
48. Roy, S.; Blackburn, E.; Valvidares, S.M.; Fitzsimmons, M.R.; Vogel, S.C.; Khan, M.; Dubenko, I.; Stadler, S.; Ali, N.; Sinha, S.K.; et al. Delocalization and hybridization enhance the magnetocaloric effect in Cu-doped Ni₂ MnGa. *Phys. Rev. B Condens. Matter. Mater. Phys.* **2009**, *79*, 1–5. [[CrossRef](#)]
49. Brown, P.J.; Gandy, A.P.; Ishida, K.; Kainuma, R.; Kanomata, T.; Neumann, K.U.; Oikawa, K.; Ouladdiaf, B.; Ziebeck, K.R.A. The magnetic and structural properties of the magnetic shape memory compound Ni₂Mn_{1.44}Sn_{0.56}. *J. Phys. Condens. Matter.* **2006**, *18*, 2249–2259. [[CrossRef](#)]
50. Mañosa, L.; Moya, X.; Planes, A.; Krenke, T.; Acet, M.; Wassermann, E.F. Ni-Mn-based magnetic shape memory alloys: Magnetic properties and martensitic transition. *Mater. Sci. Eng. A* **2008**, *481–482*, 49–56. [[CrossRef](#)]
51. Brown, P.J.; Kanomata, T.; Neumann, K.; Neumann, K.U.; Ouladdiaf, B.; Sheikh, A.; Ziebeck, K.R.A. Atomic and magnetic order in the shape memory alloy Mn₂NiGa. *J. Phys. Condens. Matter* **2010**, *22*, 506001. [[CrossRef](#)] [[PubMed](#)]
52. Mukadam, M.D.; Yusuf, S.M.; Bhatt, P. Tuning the magnetocaloric properties of the Ni₂ × Mn_{1 – X} Sn Heusler alloys. *J. Appl. Phys.* **2013**, *113*, 1–6. [[CrossRef](#)]
53. Lelièvre-Berna, E.; Bourgeat-Lami, E.; Gibert, Y.; Kernavanois, N.; Locatelli, J.; Mary, T.; Pastrello, G.; Petukhov, A.; Pujol, S.; Rouques, R.; et al. ILL polarised hot-neutron beam facility D3. In *Physica B: Condensed Matter*; Elsevier: North-Holland, The Netherlands, 2005; Volume 356, pp. 141–145.
54. Goldman, A.I. Neutron Techniques. In *Characterization of Materials*; Kaufmann, E.N., Ed.; John Wiley & Sons: Hoboken, NJ, USA, 2002; pp. 2192–2204. [[CrossRef](#)]
55. Chmielus, M. Composition, Structure and Magneto-Mechanical Properties of Ni-Mn-Ga Magnetic Shape-Memory Alloys. Ph.D. Thesis, Technische Universität Berlin, Berlin, Germany, 2010. [[CrossRef](#)]
56. Long, G.J. Neutron Diffraction. In *Comprehensive Coordination Chemistry II*; Clarendon Press: Wotton-under-Edge, UK, 2004; Volume 2.
57. Artioli, G. Single-crystal neutron diffraction. *Eur. J. Mineral* **2002**, *14*, 233–239. [[CrossRef](#)]
58. Rodríguez-Carvajal, J. Recent advances in magnetic structure determination by neutron powder diffraction. *Phys. B Condens. Matter* **1993**, *192*, 55–69. [[CrossRef](#)]
59. Glavatsky, I.; Glavatska, N.; Dobrinsky, A.; Hoffmann, J.U.; Söderberg, O.; Hannula, S.P. Crystal structure and high-temperature magnetoplasticity in the new Ni-Mn-Ga-Cu magnetic shape memory alloys. *Scr. Mater.* **2007**, *56*, 565–568. [[CrossRef](#)]
60. Brown, P.J.; Gandy, A.P.; Ishida, K.; Kainuma, R.; Kanomata, T.; Morito, H.; Neumann, K.U.; Oikawa, K.; Ziebeck, K.R.A. Crystal structures and magnetization distributions in the field dependent ferromagnetic shape memory alloy Ni₅₄Fe₁₉Ga₂₇. *J. Phys. Condens. Matter* **2007**, *19*, 016201. [[CrossRef](#)]
61. Glavatsky, I.; Glavatska, N.; Urubkov, I.; Hoffman, J.U.; Bourdarot, F. Crystal and magnetic structure temperature evolution in Ni-Mn-Ga magnetic shape memory martensite. *Mater. Sci. Eng. A* **2008**, *481–482*, 298–301. [[CrossRef](#)]
62. Molnar, P.; Sittner, P.; Lukas, P.; Hannula, S.P.; Heczko, O. Stress-induced martensite variant reorientation in magnetic shape memory Ni-Mn-Ga single crystal studied by neutron diffraction. *Smart Mater. Struct.* **2008**, *17*, 035014. [[CrossRef](#)]
63. Chmielus, M.; Glavatsky, I.; Hoffmann, J.U.; Chernenko, V.A.; Schneider, R.; Müllner, P. Influence of constraints and twinning stress on magnetic field-induced strain of magnetic shape-memory alloys. *Scr. Mater.* **2011**, *64*, 888–891. [[CrossRef](#)]
64. Chmielus, M.; Rolfs, K.; Wimpory, R.; Reimers, W.; Müllner, P.; Schneider, R. Effects of surface roughness and training on the twinning stress of Ni-Mn-Ga single crystals. *Acta Mater.* **2010**, *58*, 3952–3962. [[CrossRef](#)]
65. Chmielus, M.; Witherspoon, C.; Wimpory, R.C.; Paulke, A.; Hilger, A.; Zhang, X.; Dunand, D.C.; Müllner, P. Magnetic-field-induced recovery strain in polycrystalline Ni-Mn-Ga foam. *J. Appl. Phys.* **2010**, *108*. [[CrossRef](#)]
66. Kabra, S.; Kelleher, J.; Kockelmann, W.; Gutmann, M.; Tremsin, A. Energy-dispersive neutron imaging and diffraction of magnetically driven twins in a Ni₂MnGa single crystal magnetic shape memory alloy. *J. Phys. Conf. Ser.* **2016**, *746*, 012056. [[CrossRef](#)]
67. Hicks, T.J. Experiments with neutron polarization analysis. *Adv. Phys.* **1996**, *45*, 243–298. [[CrossRef](#)]

68. Brown, P.J.; Bargawi, A.Y.; Crangle, J.; Neumann, K.U.; Ziebeck, K.R.A. Direct observation of a band Jahn-Teller effect in the martensitic phase transition of Ni₂MnGa. *J. Phys. Condens. Matter* **1999**, *11*, 4715–4722. [[CrossRef](#)]
69. Pramanick, A.; Glavic, A.; Samolyuk, G.; Aczel, A.A.; Lauter, V.; Ambaye, H.; Gai, Z.; Ma, J.; Stoica, A.D.; Stocks, G.M.; et al. Direct in situ measurement of coupled magnetostructural evolution in a ferromagnetic shape memory alloy and its theoretical modeling. *Phys. Rev. B Condens. Matter Mater. Phys.* **2015**, *92*, 1–12. [[CrossRef](#)]
70. Lázpita, P.; Barandiarán, J.M.; Gutiérrez, J.; Mondelli, C.; Sozinov, A.; Chernenko, V.A. Polarized Neutron Study of Ni-Mn-Ga Alloys: Site-Specific Spin Density Affected by Martensitic Transformation. *Phys. Rev. Lett.* **2017**, *119*, 155701. [[CrossRef](#)]
71. Heenan, R.K.; Rogers, S.E.; Turner, D.; Terry, A.E.; Treadgold, J.; King, S.M. Small angle neutron scattering using sans2d. *Neutron News* **2011**, *22*, 19–21. [[CrossRef](#)]
72. Boothroyd, A.T. The effect of gravity on the resolution of small-angle neutron scattering. *J. Appl. Crystallogr.* **1989**, *22*, 252–255. [[CrossRef](#)]
73. Antony, A.; Schmerl, N.M.; Sokolova, A.; Mahjoub, R.; Fabijanic, D.; Stanford, N.E. Quantification of the dislocation density, size, and volume fraction of precipitates in deep cryogenically treated martensitic steels. *Metals* **2020**, *10*, 1561. [[CrossRef](#)]
74. Runov, V.V.; Chernenkov, Y.P.; Runova, M.K.; Gavriljuk, V.G.; Glavatska, N.I. Study of phase transitions and mesoscopic magnetic structure in Ni-Mn-Ga by means of small-angle polarized neutron scattering. *Phys. B Condens. Matter* **2003**, *335*, 109–113. [[CrossRef](#)]
75. Runov, V.; Runova, M.; Gavriljuk, V.; Glavatska, N. Observation of magnetic-nuclear cross-correlations in Ni-Mn-Ga. *Phys. B Condens. Matter* **2004**, *350*, 87–89. [[CrossRef](#)]
76. Sun, L.Y.; Vasin, R.N.; Islamov, A.K.; Bobrikov, I.A.; Cifre, J.; Golovin, I.S.; Balagurov, A.M. Influence of spinodal decomposition on structure and thermoelastic martensitic transition in MnCuAlNi alloy. *Mater. Lett.* **2020**, *275*, 128069. [[CrossRef](#)]
77. Sun, L.; Sumnikov, S.V.; Islamov, A.K.; Vasin, R.N.; Bobrikov, I.A.; Balagurov, A.M.; Cheng, W.; Churyumov, Y.; Golovin, I.S. Spinodal decomposition influence of austenite on martensitic transition in a Mn-13 at.%Cu alloy. *J. Alloys Compd.* **2021**, *853*, 157061. [[CrossRef](#)]
78. Benacchio, G.; Titov, I.; Malyeyev, A.; Peral, I.; Bersweiler, M.; Bender, P.; Mettus, D.; Honecker, D.; Gilbert, E.P.; Coduri, M.; et al. Evidence for the formation of nanoprecipitates with magnetically disordered regions in bulk Ni₅₀Mn₄₅In₅ Heusler alloys. *Phys. Rev. B* **2019**, *99*, 184422. [[CrossRef](#)]
79. Sarkar, S.K.; Ahlawat, S.; Kaushik, S.D.; Babu, P.D.; Sen, D.; Honecker, D.; Biswas, A. Magnetic ordering of the martensite phase in Ni-Co-Mn-Sn-based ferromagnetic shape memory alloys. *arXiv* **2019**, arXiv:1908.08860v2. [[CrossRef](#)]
80. Kopitsa, G.P.; Runov, V.V.; Grigoriev, S.V.; Bliznuk, V.V.; Gavriljuk, V.G.; Glavatska, N.I. The investigation of Fe-Mn-based alloys with shape memory effect by small-angle scattering of polarized neutrons. *Phys. B Condens. Matter* **2003**, *335*, 134–139. [[CrossRef](#)]
81. Bliznuk, V.V.; Gavriljuk, V.G.; Kopitsa, G.P.; Grigoriev, S.V.; Runov, V.V. Fluctuations of chemical composition of austenite and their consequence on shape memory effect in Fe-Mn-(Si, Cr, Ni, C, N) alloys. *Acta Mater.* **2004**, *52*, 4791–4799. [[CrossRef](#)]
82. Webster, J.R.P.; Langridge, S.; Dalglish, R.M.; Charlton, T.R. Reflectometry techniques on the second target station at ISIS: Methods and science. *Eur. Phys. J. Plus* **2011**, *126*, 1–5. [[CrossRef](#)]
83. Daillant, J.; Gibaud, A. *X-Ray and Neutron Reflectivity: Principles and Applications*; Springer: Berlin/Heidelberg, Germany, 1999.
84. Tolan, M.; Press, W. X-ray and neutron reflectivity. *Z. Fur Krist.* **1998**, *213*, 319–336. [[CrossRef](#)]
85. Khaydukov, Y.N.; Kravtsov, E.A.; Zhaketov, V.D.; Progliado, V.V.; Kim, G.; Nikitenko, Y.V.; Keller, T.; Ustinov, V.V.; Aksenov, V.L.; Keimer, B. Magnetic proximity effect in Nb/Gd superlattices seen by neutron reflectometry. *Phys. Rev. B* **2019**, *99*, 3–7. [[CrossRef](#)]
86. Singh, S.; Swain, M.; Basu, S. Kinetics of interface alloy phase formation at nanometer length scale in ultra-thin films: X-ray and polarized neutron reflectometry. *Prog. Mater. Sci.* **2018**, *96*, 1–50. [[CrossRef](#)]
87. Granovsky, S.; Gaidukova, I.; Sokolov, A.; Devishvili, A.; Snegirev, V. Structural and magnetic properties of Ni₅₀Mn₃₅In₁₅ thin films. *Solid State Phenom.* **2015**, *233–234*, 666–669. [[CrossRef](#)]
88. Hussey, D.S.; Bocker, C.; Cook, J.C.; Jacobson, D.L.; Gentile, T.R.; Chen, W.C.; Baltic, E.; Baxter, D.V.; Doskow, J.; Arif, M. A New Cold Neutron Imaging Instrument at NIST. In *Physics Procedia*; Elsevier B.V.: Amsterdam, The Netherlands, 2015; Volume 69, pp. 48–54.
89. Wenk, H.R.; Kern, H.; Schaefer, W.; Will, G. Comparison of neutron and X-ray diffraction in texture analysis of deformed carbonate rocks. *J. Struct. Geol.* **1984**, *6*, 687–692. [[CrossRef](#)]
90. Matthies, S.; Pehl, J.; Wenk, H.R.; Lutterotti, L.; Vogel, S.C. Quantitative texture analysis with the HIPPO neutron TOF diffractometer. *J. Appl. Crystallogr.* **2005**, *38*, 462–475. [[CrossRef](#)]
91. Brokmeier, H.G.; Gan, W.M.; Randau, C.; Völler, M.; Rebelo-Kornmeier, J.; Hofmann, M. Texture analysis at neutron diffractometer STRESS-SPEC. *Nucl. Instrum. Methods Phys. Res. Sect. A Accel. Spectrometers Detect. Assoc. Equip.* **2011**, *642*, 87–92. [[CrossRef](#)]
92. Nie, Z.H.; Wang, Y.D.; Wang, G.Y.; Richardson, J.W.; Wang, G.; Liu, Y.D.; Liaw, P.K.; Zuo, L. Phase transition and texture evolution in the Ni-Mn-Ga ferromagnetic shape-memory alloys studied by a neutron diffraction technique. *Metall. Mater. Trans. A Phys. Metall. Mater. Sci.* **2008**, *39*, 3113–3119. [[CrossRef](#)]
93. Chulist, R.; Poetschke, M.; Boehm, A.; Brokmeier, H.G.; Garbe, U.; Lippmann, T.; Oertel, C.G.; Skrotzki, W. Cast and rolling textures of NiMnGa alloys. *Mater. Res. Soc. Symp. Proc.* **2008**, *1050*, 30–35. [[CrossRef](#)]
94. Winkler, B. Applications of neutron radiography and neutron tomography. *Rev. Mineral. Geochem.* **2006**, *63*, 459–471. [[CrossRef](#)]
95. Woracek, R.; Penumadu, D.; Kardjilov, N.; Hilger, A.; Boin, M.; Banhart, J.; Manke, I. 3D mapping of crystallographic phase distribution using energy-selective neutron tomography. *Adv. Mater.* **2014**, *26*, 4069–4073. [[CrossRef](#)] [[PubMed](#)]

96. Samothrakitis, S.; Larsen, C.B.; Woracek, R.; Heller, L.; Kopeček, J.; Gerstein, G.; Maier, H.J.; Rameš, M.; Tovar, M.; Šittner, P.; et al. A multiscale study of hot-extruded CoNiGa ferromagnetic shape-memory alloys. *Mater. Des.* **2020**, *196*, 109118. [[CrossRef](#)]
97. Jiménez-Ruiz, M.; Ivanov, A.; Fuard, S. LAGRANGE—The new neutron vibrational spectrometer at the ILL. *J. Phys. Conf. Ser.* **2014**, *549*, 012004. [[CrossRef](#)]
98. Eckert, J. Theoretical introduction to neutron scattering spectroscopy. *Spectrochim. Acta Part A Mol. Spectrosc.* **1992**, *48*, 271–283. [[CrossRef](#)]
99. Hudson, B.S. Inelastic Neutron Scattering: A Tool in Molecular Vibrational Spectroscopy and a Test of ab Initio Methods. *J. Phys. Chem. A* **2001**, *105*, 3949–3960. [[CrossRef](#)]
100. Zheludev, A.; Shapiro, S.M.; Wochner, P.; Schwartz, A.; Wall, M.; Tanner, L.E. Phonon anomaly, central peak, and microstructures in Ni₂MnGa. *Phys. Rev. B* **1995**, *51*, 11310–11314. [[CrossRef](#)] [[PubMed](#)]
101. Zheludev, A.; Shapiro, S.; Wochner, P.; Tanner, L. Precursor effects and premartensitic transformation in MnGa. *Phys. Rev. B Condens. Matter Mater. Phys.* **1996**, *54*, 15045–15050. [[CrossRef](#)]
102. Recarte, V.; Pérez-Landazábal, J.I.; Sánchez-Alarcos, V.; Cesari, E.; Jiménez-Ruiz, M.; Schmalzl, K.; Chernenko, V.A. Direct evidence of the magnetoelastic interaction in Ni₂MnGa magnetic shape memory system. *Appl. Phys. Lett.* **2013**, *102*, 1–5. [[CrossRef](#)]
103. Moya, X.; González-Alonso, D.; Mañosa, L.; Planes, A.; Garlea, V.O.; Lograsso, T.A.; Schlagel, D.L.; Zarestky, J.L.; Aksoy, S.; Acet, M. Lattice dynamics in magnetic superelastic Ni-Mn-In alloys: Neutron scattering and ultrasonic experiments. *Phys. Rev. B Condens. Matter Mater. Phys.* **2009**, *79*, 214118. [[CrossRef](#)]
104. Moya, X.; Mañosa, L.; Planes, A.; Krenke, T.; Acet, M.; Garlea, V.O.; Lograsso, T.A.; Schlagel, D.L.; Zarestky, J.L. Lattice dynamics and phonon softening in Ni-Mn-Al Heusler alloys. *Phys. Rev. B Condens. Matter Mater. Phys.* **2006**, *73*, 64303. [[CrossRef](#)]